ORIENTATION-PREFERENTIAL GROWTH DURING SECONDARY RECRYSTALLIZATION IN AA5182 SHEET

*Yusuke Yamamoto and Mineo Asano

Research and Development Division, UACJ Corporation
Nagoya, Aichi, Japan
*(*Corresponding author: yamamoto-yusuke@uacj.co.jp)*

ABSTRACT

The present study investigated the texture transition during secondary recrystallization in the AA5182 sheet. During the initial stage of annealing, the texture showed a weak Cube orientation as the primary recrystallization texture. During the secondary recrystallization with abnormal grain growth, the area ratio of the {hkl} <011> orientations increased by consuming the other orientations. The texture transition was calculated by the 2-D Monte Carlo simulation with the misorientation dependency. When the higher grain boundary mobility was set in the specific range of the high angle misorientation, the orientation preferential growth of the RW {100} <011> orientation was reproduced. However, other {hkl} <110> orientations could not be well reproduced by the misorientation dependency.

KEYWORDS

Al-Mg alloy, AA5182, Secondary recrystallization, Abnormal grain growth, Grain boundary mobility

INTRODUCTION

Crystal orientation and texture are important factors for aluminum sheet products from the standpoint of mechanical property, formability and isotropy. The recrystallization texture results from the orientation preferential growth from the rolling deformation microstructure and the texture (Alvi, Cheong, Suni, Weiland, & Rollett, 2008). Texture development has been a topic of intense research for decades with advances in analysis methods, e.g., orientation mapping (OIM) and computer simulations (Fjeldberg & Marthinsen, 2010; Ivasishin, Shevchenko, Vasiliev, & Semiatin, 2006). The grain boundary characteristic is considered to be a key for the orientation preferential growth. In the case of the recrystallization from the deformed microstructure, not only the grain boundary characteristic, but also the dislocation density and the subgrain size affect the nucleation and the grain growth (Engler, Löchte, & Hirsch, 2007). On the other hand, in the case of secondary recrystallization, the dislocation density and the subgrain size can be ignored and the effect of the grain boundary characteristic can play a significant role in the grain growth.

There is intense research about the texture development during secondary recrystallization in aluminum alloys and it was reported that coarse {hkl} <011> grains were formed during the secondary recrystallization (Suk, Shin, & Huh, 2006; Rios, & Gottstein, 2001). However, the mechanism of forming the {hkl} <011> grains has not been fully clarified. In the present study, the effect of the grain boundary characteristic on the orientation preferential growth was investigated by EBSD analysis and Monte-Carlo (MC) simulation.

EXPERIMENTAL

Table 1 shows the chemical composition of a cold-rolled sheet of AA5182 aluminum. The cold-rolled sheet with a 1.0 mm thickness was prepared by direct chill casting, homogenizing, hot rolling and cold rolling. The cold-rolled sheets were cut into 35mm wide and 200mm long sheets, parallel to the rolling direction. The sheets were annealed in an infrared heating furnace until the test piece reached 773K (Stage I), 783K (Stage II) and 798K (Stage III). After cutting out a 0.25mm thick piece from the surface of the annealed sheet, the cut surface was polished for EBSD measurement. The EBSD measurement was carried out in an area of 3mm × 3mm by 3μm step. By using the EBSD raw data, an MC simulation was used to evaluate the contribution of the grain boundary characteristic to the orientation preferential growth.

Table 1. Chemical composition of specimens. (mass%)

Si	Fe	Cu	Mn	Mg	Cr	Zn	Ti	Al
0.1	0.2	0.0	0.3	4.8	Tr.	Tr.	0.02	Bal.

RESULTS

Figure 1 shows the grain direction maps at each annealing stage. The grain direction against the rolling direction is classified by the colors of black for the <001> direction and gray for the <011> direction, allowing a 15° misorientation from the ideal direction. The Stage I grain structure consisted of only fine grains towards both the <001> and <011> directions as shown in Figure 1a. In Stage I, the area ratio of the black grains was slightly larger than that of the gray grains. The Stage II grain structure consisted of fine grains and some coarse grains as shown in Figure 1b. The gray grains occupied the majority of the coarsened grains. The Stage III grain structure consisted of extra coarse grains, coarse grains and fine grains as shown in Figure 1c. All the extra coarse grains were the gray grains.

The Orientation Distribution Function (ODF) of the annealed sheet was calculated in order to understand the orientation texture transition at each annealing stage. Figure 2 shows the φ2 cross section maps of the ODF at Stage I and Stage III. Figure 2a indicates that in Stage I, the annealed sheet had a weak Cube {001} <100> texture as the primary recrystallization texture. In Stage III, the {100} <011>, {411} <011> and {011} <011> textures appeared as the result of the abnormal grain growth during the secondary recrystallization. The {hkl} <110> texture seemed to distribute from {001} <110> in the φ2 = 0° cross section to {411} <110> in the φ2 = 45° cross section as a fiber-like distribution. In the fiber-like distribution, the highest intensity was the A orientation; (φ1, Φ, φ2) = (10°, 20°, 35°).
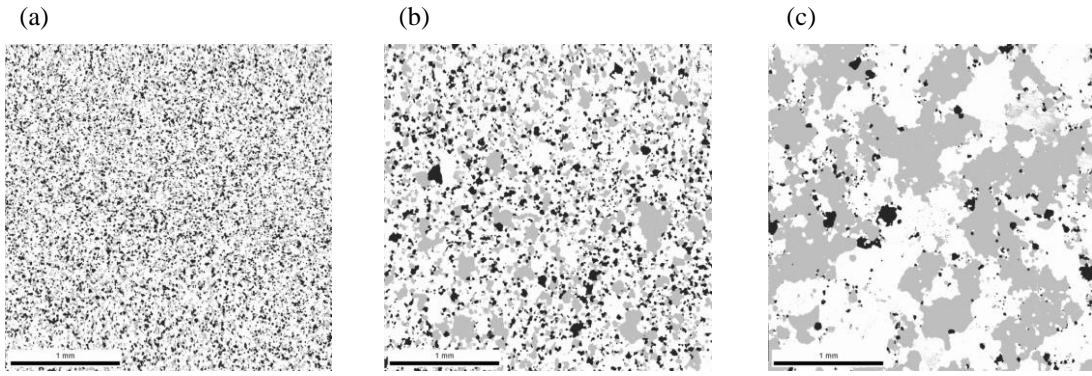
Figure 1. The crystal direction maps during each annealing stage. (a) Stage I, (b) Stage II, (c) Stage III.
Black area denotes the grains which have a <001> direction toward the rolling direction.
Gray area denotes the grains which have a <011> direction toward the rolling direction.
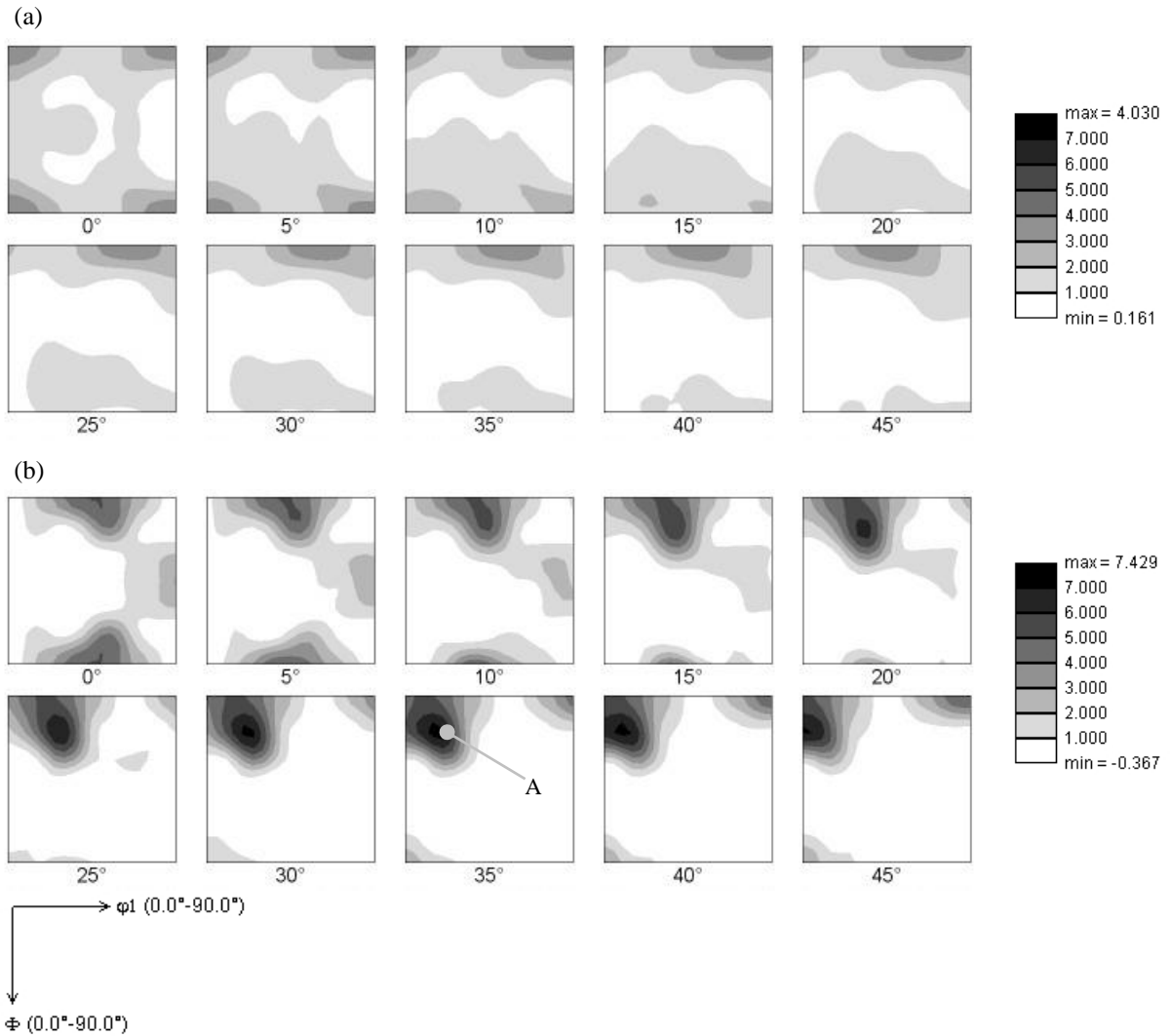Both colors allow a 15° misorientation from the ideal direction.

(a)

(b)

Figure 2. φ2 cross section maps of the Orientation Distribution Function: (a) Stage I. (b) Stage III.

Figure 3 shows the transition of the grain size distribution of each crystal orientation. As a typical orientation, the Cube orientation and A orientation were selected to understand the grain growth behavior. The Cube orientation grains gradually grew and disappeared during the annealing process from Stage I to Stage III. The A orientation grains also gradually grew during the annealing process. However, simultaneously, some grains started abnormal growth around Stage II and the abnormal grain growth dominated the grain growth process in Stage III.

(a)

(b)

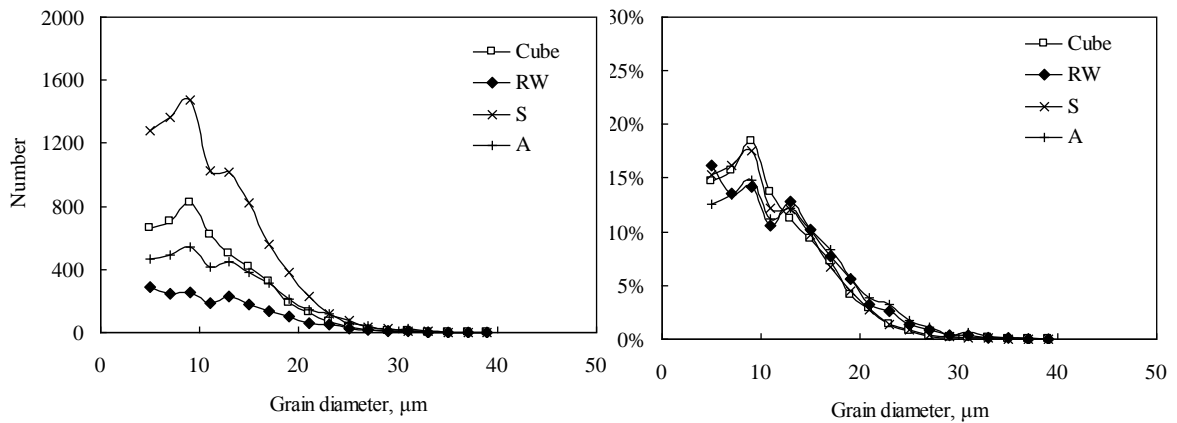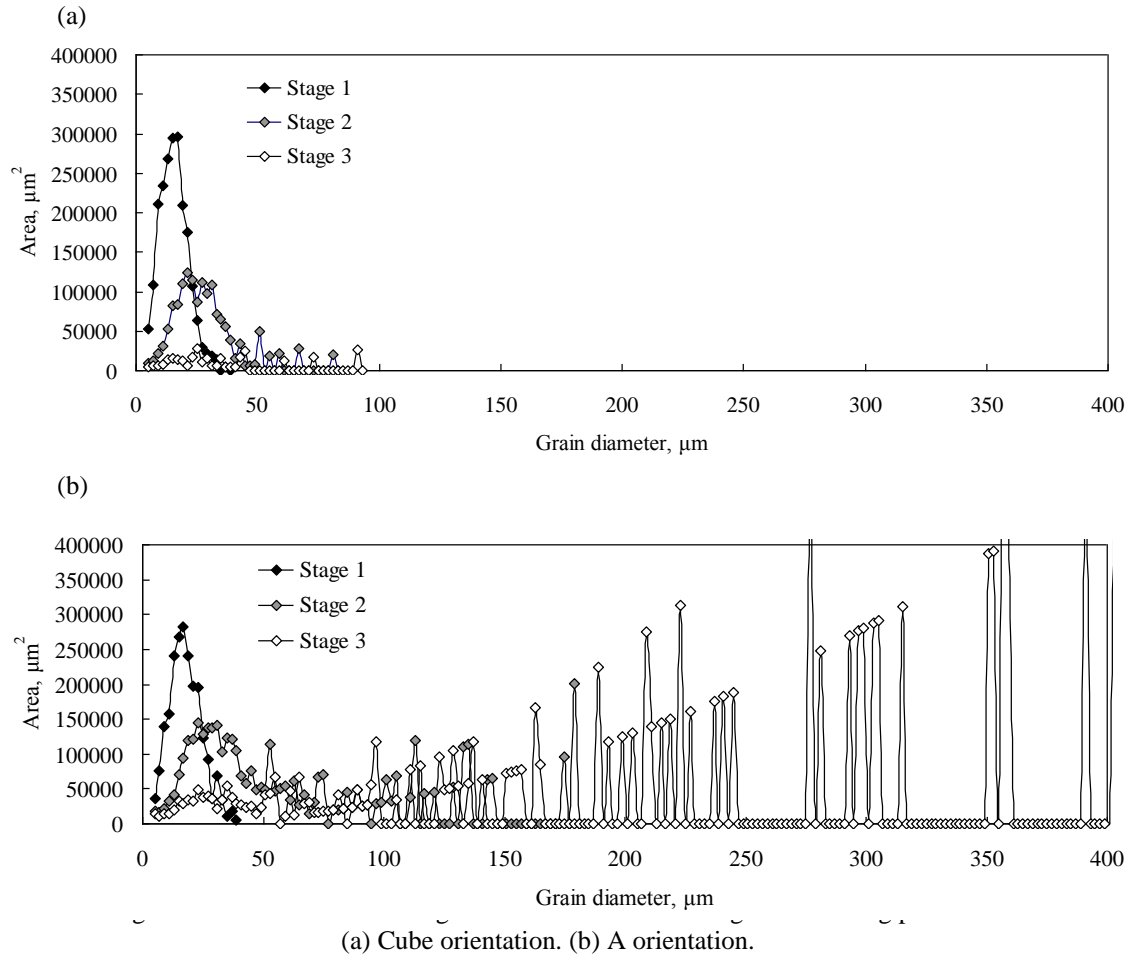(a) Cube orientation. (b) A orientation.

Figure 4. The grain size distribution of the Cube (□), RW (◆), S (×) and A (+) orientations.

The orientation preferential growth of the {hkl} <110> orientations were first considered to be the effect of the size priority after the primary recrystallization process in Stage I. Figure 4 shows the grain size distribution of the main orientations. There is a difference from the standpoint of the grain number, but no orientation showed a size priority compared to the grain size distribution of the other orientations from the standpoint of the ordered ratio of the grain number, thus the orientation preferential growth was reconsidered to be the effect of the grain boundary mobility dependency of the misorientation between the coarsened grains and the initial texture in Stage I.

It is difficult to directly observe abnormal grain growth by repeating the EBSD measurement in the several annealing steps because abnormal grain growth could occur from behind the measuring cross section and the grains tend to be too coarse to understand the growth mechanism during the early stage of the abnormal grain growth. In the present study, a 2-D MC simulation was used to reproduce the orientation preferential growth and better understand the mechanism of the orientation preferential growth.

The grain boundary energy anisotropy is characterized by a plateau for the high-angle boundaries and by the Read-Shockley formula for the small angle boundaries (Ma, Kazaryan, Dregia, & Wang, 2004):

$$E(\theta) = \begin{cases} E_0 \cdot \left(1 - \ln\left(\dfrac{\theta}{\theta_m} \right) \right) & \theta < \theta_m \\ E_0 & \theta \geq \theta_m \end{cases} \tag{1}$$

where θ_m is the maximum angle at which the Read-Shockler equation still holds, and E_0 is a constant value. $15°$ was used for the θ_m value in this study. Correspondingly, the mobility anisotropy is characterized by

$$M(\theta) = \begin{cases} M_0 \cdot \left(1 - \exp\left(\dfrac{-\theta}{\theta_m} \right)^7 \right) & \theta < 15° \\ M_0 \cdot \left(1 - \exp\left(\dfrac{-\theta}{\theta_m} \right)^7 \right) + M_0 \cdot \left(1 - \exp\left(\dfrac{-(\theta-15)}{\theta_m} \right)^7 \right) & 15° \leq \theta < 42.5° \\ M_0 \cdot \left(1 - \exp\left(\dfrac{-\theta}{\theta_m} \right)^7 \right) + M_0 \cdot \left(1 - \exp\left(\dfrac{-(60-\theta)}{\theta_m} \right)^7 \right) & 42.5° \leq \theta < 70° \\ M_0 & 70° \geq \theta \end{cases} \tag{2}$$

where M_0 is a constant. Note that the magnitude of θ_m determines the degree of anisotropy and it is assumed to be $20°$ in this simulation. An approach similar to that used by Ivasishin et al. (Ivasishin, Shevchenko, Vasiliev, & Semiatin, 2006). The misorientation dependency of the boundary energy and mobility described by Equations (1) and (2) are shown in Figure 5.
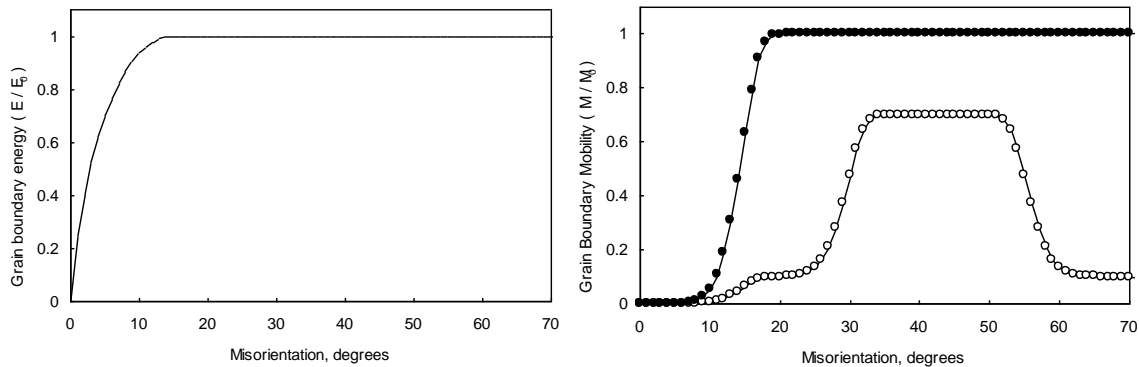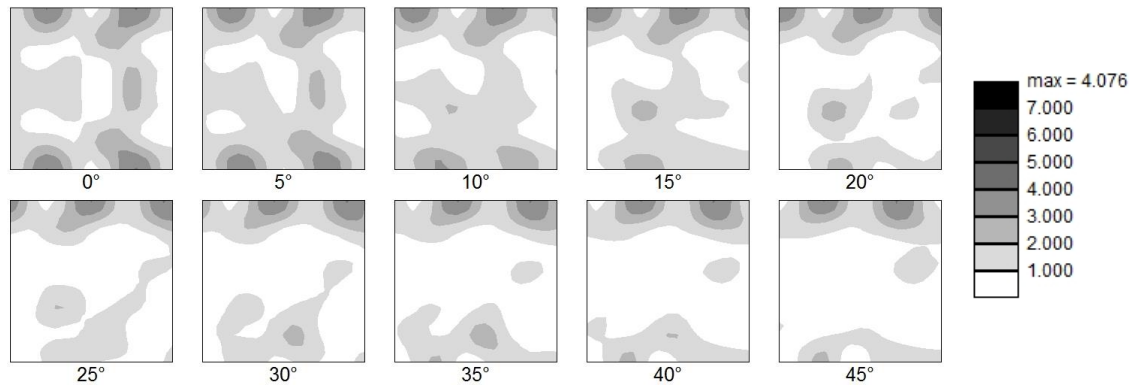

Figure 5. The misorientation dependency of the grain boundary energy and mobility described by Equations (1) and (2). (a) The grain boundary energy. (b) The grain boundary mobility with the dependency of only the low angle misorientation (●) and with the dependency for both the low and high angle misorientations (○).

The MC model domain was formed by a 2-D cubic array of Monte-Carlo Units (MUs), each of which represented a point in a cubic lattice. The length of the side of the model domain was set equal to 250 MUs. The initial texture for the MC simulation was obtained from the EBSD raw data in Stage I. Each unit was characterized by its set of Euler angles. The total grain boundary energy in eachof the MUs was calculated according to Equation (1). The possible new MU's orientations were four orientations of four adjacent grains. The probability of reorientation to a new orientation was:
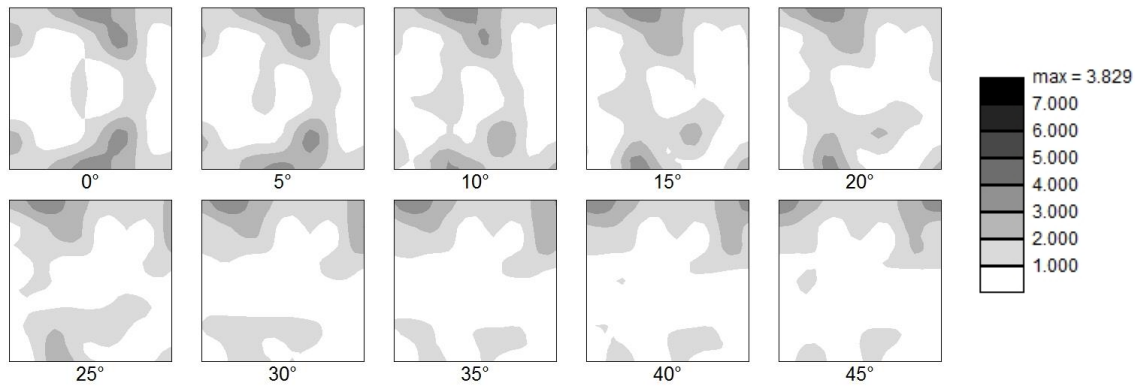
$$P = \frac{\Delta E_{total}}{E_0} \cdot \frac{M}{M_0} \tag{3}$$

where $\triangle E_{total}$ is the difference in the total grain boundary energy between the original MU and an adjacent MU, and M is the grain boundary mobility between the original MU and an adjacent MU. The new orientation was determined according to the probability of the possible four orientations given by Equation (3).

(a)

(b)

Figure 6. φ2 cross section maps of Orientation Distribution Function:
(a) With the dependency of only the low angle misorientation.
(b) With the dependency of both the low and high angle misorientations.

The calculated texture by the present MC simulation is shown in Figure 6. When considering the dependency of the low angle misorientation on only the grain boundary mobility, the calculated texture shown in Figure 6a was similar to the texture of the primary recrystallization in Stage I as shown in Figure 2a and it did not reproduce the texture after orientation preferential growth during the secondary recrystallization in Stage III as shown in Figure 2b. On the other hand, when considering both the dependency of the low angle

and high angle misorientations shown in Figure 5b, the texture of the RW {100} <011> orientation appeared after 300 MCS in Figure 6b. However, the intensity of the A orientation and {411} <011> orientation were not as high as that expected. The misorientation dependency of the high angle misorientation on the grain boundary mobility expresses the difference in the pinning force mainly by the Mn addition to the AA5182 sheet at the grain boundary. In the range of the 30-50° misorientation, major Coincidence Site Lattice (CSL) boundaries like Σ5, Σ7, Σ9 and Σ11 are included. CSL grain boundaries were reported to have a higher grain boundary mobility compared to the other grain boundaries (Ushigami, Kumano, Haratani, Nakamura, Takebayashi, & Kubota, 2004). To simply consider the effect of the CSL boundary mobility, the higher mobility in the range of the 30–50° misorientation was adopted. The assumption of the misorientation dependency of the grain boundary explained the RW {100} <011> orientation appearance, but the description of the misorientation dependency on grain boundary mobility was not detailed enough to perfectly reproduce the orientation preferential growth. The misorientation dependency of the grain boundary mobility for each axis, at least the <001>, <011> and <111> axes, would be necessary to correctly describe the effect of the CSL grain boundary and to reproduce the texture transition during the secondary recrystallization.

CONCLUSIONS

The texture transition during the secondary recrystallization in the AA5182 sheet was investigated. During the initial stage of annealing, the texture showed a weak Cube orientation. During the abnormal grain growth, the area ratio of the {hkl} <011> orientations increased by consuming the other orientations. The grain boundary mobility between the consumed grains and the coarsened grains were calculated by the 2-D MC simulation with the misorientation dependency. When the high grain boundary mobility was set in the specific range of a high angle misorientation, the orientation preferential growth of the RW {100} <011> orientation was reproduced. However, other {hkl} <011> orientations could not be well reproduced by the present misorientation dependency. The misorientation dependency of the grain boundary mobility for each axis would be necessary to correctly describe the effect of the CSL grain boundary and to reproduce the texture transition during the secondary recrystallization.

REFERENCES

Alvi, M. H., Cheong, S. W., Suni, J. P., Weiland, H. & Rollett, A. D. (2008). Cube texture in hot-rolled aluminum alloy 1050 (AA1050)-nucleation and growth behavior. *Acta Materialia*, 56, 3098–3108.

Engler, O., Löchte, L. & Hirsch, J. (2007). Through-process simulation of texture and properties during the thermomechanical processing of aluminium sheets. *Acta Materialia*, 55, 5449–5463.

Fjeldberg, E., & Marthinsen K. (2010). A 3D Monte Carlo study of the effect of grain boundary anisotropy and particles on the size distribution of grains after recrystallization and grain growth. *Computional Material Science*, 48, 267–281.

Ivasishin, O. M., Shevchenko, S. V., Vasiliev, N. L., & Semiatin, S. L. (2006). A 3-D Monte-Carlo (Potts) model for recrystallization and grain growth in polycrystalline materials. *Material Science and Engineering A*, 443, 216–232.

Ma, N., Kazaryan, A., Dregia, S. A., & Wang, Y. (2004). Computer simulation of texture evolution during grain growth: effect of boundary properties and initial microstructure. *Acta Materialia*, 52, 3869–3879.

Rios, P. R., & Gottstein, G. (2001). Texture evolution during normal and abnormal grain growth in an Al-1 wt% Mn alloy. *Acta Materialia*, 49, 2511–2518.

Suk, H. G., Shin, E. J., & Huh, M. Y. (2006). Development of abnormal grain growth in cold rolled and recrystallized AA 5182 sheet. *Solid State Phenomena*, 116–117, 316–319.

Ushigami, Y., Kumano, T., Haratani, T., Nakamura, S., Takebayashi, S., & Kubota, T. (2004). Secondary Recrystallization in Grain-Oriented Silicon Steel. *Material Science Forum*, 467–470, 853–862.